Soft Matter

PAPER

View Article Online
View Journal

Cite this: DOI: 10.1039/d3sm00014a

Coupled bond dynamics alters relaxation in polymers with multiple intrinsic dissociation rates†

Robert J. Wagner [a] and Franck J. Vernerey *[b]

Received 4th January 2023,
Accepted 16th March 2023

DOI: 10.1039/d3sm00014a

rsc.li/soft-matter-journal

Dynamic networks containing multiple bond types within a continuous network grant engineers another design parameter – relative bond fraction – by which to tune storage and dissipation of mechanical energy. However, the mechanisms governing emergent properties are difficult to deduce experimentally. Therefore, we here employ a network model with prescribed fractions of dynamic and stable bonds to predict relaxation characteristics of hybrid networks. We find that during stress relaxation, predominantly dynamic networks can exhibit long-term moduli through conformationally inhibited relaxation of stable bonds due to exclusion interactions with neighboring chains. Meanwhile, predominantly stable networks exhibit minor relaxation through non-affine reconfiguration of dynamic bonds. Given this, we introduce a single fitting parameter, ξ, to Transient Network Theory *via* a coupled rule of mixture, that characterizes the extent of stable bond relaxation. Treating ξ as a fitting parameter, the coupled rule of mixture's predicted stress response not only agrees with the network model's, but also unveils likely micromechanical traits of gels hosting multiple bond dissociation timescales.

1. Introduction

Networked polymeric materials containing multiple bond types have become increasingly investigated for their exemplary combinations of mechanical strength and toughness.[1–5] Many state-of-the-art polymers contain both relatively stable covalent bonds and dynamic physical (or covalent) bonds (*e.g.*, metallo–ligand interactions, ionic bonds, hydrogen bonds, *etc.*) within the same continuous network.[6–12] In such systems, the stable bonds often form a scaffold that supports the dynamic bonds throughout the material. Under these conditions, the stable bonds may preserve suitably high moduli, while incorporation of the sacrificial or reversible dynamic bonds introduces tunable viscoelasticity[6,13–17] and self-healing ability.[9,18,19]

While designing such materials, researchers often employ physically motivated constitutive modeling techniques through which the properties of individual bonds may be used to predict the globally emergent responses of the networks.[20–23] However, real-time experimental characterization of such materials' microstructures remains exceedingly challenging and is relatively limited to techniques such as small angle neutron scattering,[24] or inference from diffusion and rheology data.[25] Therefore, gauging the degree of phenomenology in such models or interpreting their parameters is somewhat difficult, thus limiting the confidence in extrapolations made about microstructure using these approaches.

To address this limitation, many researchers have resorted to network-scale modeling to explore polymeric microstructure.[3,26–31] We here employ one such recently developed model[29] to investigate the percolation threshold of stable bonds in 2D networks containing interstitial dynamic bonds (Fig. 1). Through this model, we examine the mechanical stress response of networks containing different fractions of stable and dynamic bonds, and then relate the clustering and geometric percolation of stable bonds to the emergence of a long-term, finite stress plateau beyond which further stress relaxation is likely governed by reptation,[32] bond lifetime renormalization,[33] and other topological effects neglected by the simple 2D model.

This network model deliberately hosts just one relaxation mechanism – that of bond dynamics-driven reconfiguration – and therefore allows us to isolate the effects of bond dynamics on dissipation over intermediate experimental timescales (above short term segmental relaxation but below long term reptation[34] timescales). We find that under some topological conditions, a portion of stable bonds that are fully percolated undergo non-affine conformational relaxation due to the

[a] Sibley School of Mechanical & Aerospace Engineering, Cornell University, Ithaca, NY, USA
[b] Department of Mechanical Engineering, Program of Materials Science & Engineering, University of Colorado, Boulder, CO, USA.
E-mail: franck.vernerey@colorado.edu

† Electronic supplementary information (ESI) available: Includes (I) a detailed description of the discrete network model, (II) pertinent derivations for the TNT (continuum approach), (III) extended network modeling results for the broader parametric space. See DOI: https://doi.org/10.1039/d3sm00014a

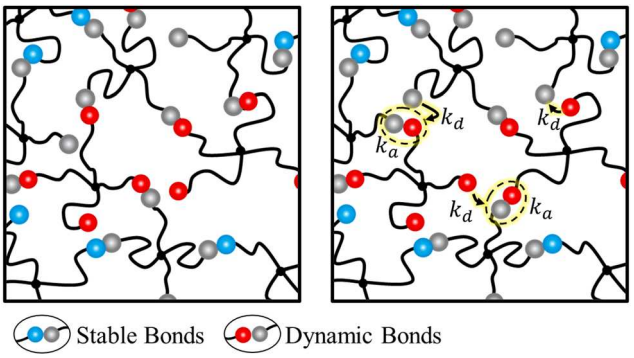

Fig. 1 Hybrid network schematic. A schematic of a dynamic network including both stable bonds (blue-to-grey) and dynamic bonds (red-to-grey) is displayed before (left) and after (right) a set of dissociation and attachment events at characteristic rates k_d and k_a, respectively.

reconfiguration of neighboring dynamic bonds. Equipped with this information we establish a coupled rule of mixture for hybrid networks using transient network theory (TNT).[23] This rule introduces just one additional, dimensionless parameter, $\xi \in [0,1]$, that characterizes the degree to which stable bonds can conformationally relax due to adjacent bond dynamics. Finally, we apply the model (in conjunction with other pertinent phenomena, such as bond lifetime renormalization,[33,35] and force-sensitive bond dissociation[36]) to predict the mechanical relaxation response of an experimental gel[6] that hosts two reversible, covalent bond types with differing intrinsic binding energies.

2. Discrete model overview

The network model used here, introduced by Wagner *et al.* (2021),[29] simulates discrete networks within 2D, periodic, representative volume elements to which deformations may be applied. For detailed methods pertaining to network initiation and spatiotemporal normalization, see ESI† Section SIA. The networks are comprised of $\mathcal{N} = 400$ (see Fig. S1, ESI† for domain size convergence results), four or eight-armed ($z \in \{4,8\}$), star-shaped macromers whose central junctions represent permanent crosslinks or "nodes" and whose free ends are functionalized with binding sites or "stickers". Either stable or dynamic telechelic bonds may form between neighboring nodes, the latter of which are assigned some constant dissociation kinetic rate, k_d. Bond association is captured through the sub-diffusive Rouse scaling utilized in Wagner *et al.* (2021),[29] that gives the attachment rate as:[33]

$$k_a = \tau_0^{-1}\left(\frac{b}{d}\right)^4, \tag{1}$$

where b is the length of a single Kuhn segment, τ_0 is the time it takes a Kuhn segment to diffuse a distance of b, and d is the pairwise separation distance between neighboring nodes having open stickers within cutoff distance $d < l_c$ (see ESI† Section SIB for details). Here, $l_c = Nb$ where N is the number of Kuhn segments in an attached chain so that l_c is its contour length. Both bond association and dissociation are treated as memoryless processes such that the probability of a reaction event occurring at time t follows:[29]

$$dP = ke^{-kt}dt, \tag{2}$$

where k represents either the rate of bond association, k_a – governed by eqn (1) – or dissociation, k_d (set *a priori*). For simplicity, attached chains are treated as ideal entropic springs that impart pairwise tensile forces on the nodes to which they are attached according to:

$$\boldsymbol{f}_t = 3k_BT\frac{\lambda}{\sqrt{N}b}\frac{\boldsymbol{r}}{|\boldsymbol{r}|}, \tag{3}$$

where k_B is the Boltzmann constant, T is the ambient temperature, $\lambda = |\boldsymbol{r}|/(\sqrt{N}b)$ is the chain stretch, and $\boldsymbol{r}$ is the end-to-end vector of a chain. Entropic forces are balanced by repulsive forces deriving from steric interactions between neighboring nodes or polymer chains. For simplicity, repulsive forces are captured *via* a phenomenological inverse potential for soft particles[37] that yields a force–distance relation of:

$$\boldsymbol{f}_r = \frac{\boldsymbol{d}}{|\boldsymbol{d}|}\begin{cases} -\gamma E\left[l_c^{-1} + (l_c)^{\gamma}d^{-(\gamma+1)}\right], & \text{if } d < l_c \\ 0, & \text{if } d \geq l_c \end{cases}, \tag{4}$$

where E is a parameter with units of energy that characterizes the extent of repulsion, $\gamma = 2$ is a scaling coefficient that modulates particle stiffness, d is the end-to-end separation vector between nodes, and $l_c = Nb$ is the cutoff distance beyond which steric interactions are impossible.

Pairwise interactions are used to compute the unbalanced force on each node, denoted by α, as $\boldsymbol{f}^{\alpha} = \sum_{\beta}\boldsymbol{f}^{\alpha\beta}$. Here, $\boldsymbol{f}^{\alpha\beta}$ represents a single pairwise force (either $\boldsymbol{f}_t$ or $\boldsymbol{f}_r$) between node α and its β-th neighbor. Assuming quasi-equilibrium, unbalanced forces are used to iteratively equilibrate each nodes position after every deformation or network reconfiguration step (*i.e.*, "timestep") using a gradient descent approach.[38] Namely, the position of node α is updated from iteration k to $k+1$ according to:

$$\boldsymbol{x}_{k+1}^{\alpha} = \boldsymbol{x}_k^{\alpha} + \eta^{-1}\boldsymbol{f}^{\alpha}, \tag{5}$$

where η is an overdamping coefficient with units of mass per time-squared set to ensure stable convergence. Note that η is not to be confused with the overdamping coefficient of Brownian dynamics models, which relates to the thermal energy, k_BT, particle diffusion coefficient, D, and differential time interval, Δt, through the Einstein relation ($\eta \sim k_BTD^{-1}\Delta t^{-1}$).[39,40] Rather, η is a numerical value set arbitrarily to ensure stable convergence to the lowest energy network conformation within each timestep on the basis of quasistatic loading conditions. After equilibration within each timestep, network stress is computed *via* the virial formula:

$$\boldsymbol{\sigma} = \frac{1}{2V}\sum_{\alpha}^{\mathcal{N}}\sum_{\beta}\boldsymbol{r}^{\alpha\beta}\otimes\boldsymbol{f}^{\alpha\beta}, \tag{6}$$

where V is the domain volume, $\boldsymbol{r}^{\alpha\beta}$ is the end-to-end vector between node α and attached neighbor β, and $\boldsymbol{f}^{\alpha\beta}$ denotes the pairwise tensile and repulsive force between said nodes.

Since the discrete model domains are periodic, rectangular volume elements, incremental changes to their four corners cause the chains that transcend the four boundaries to stretch or shorten. Accordingly, incompressible deformations may be applied by displacing the four corners of the domain. To conduct simulated stress relaxation experiments, we here apply a symmetrical velocity gradient of the form, $\boldsymbol{L} = \mathrm{diag}(-\dot{\varepsilon}, \dot{\varepsilon})$, where $\dot{\varepsilon}$ is the true strain rate. When $\dot{\varepsilon}$ is set far greater than the intrinsic bond dissociation rate, k_d, dynamic networks approach elastic behavior. Therefore, to ensure that bond dynamics are negligible during initial loading for stress relaxation experiments, we here set $\dot{\varepsilon}/k_d = 100$. The networks are strained until they reach a principal stretch of $\lambda = 2$, after which the deformation is held and stress relaxation is allowed to occur for $t^* \approx 4$ (where $t^* = tk_d$), corresponding to relaxation within 2% of the steady state value predicted by exponential decay. The applied loading history (true strain with respect to time) is depicted in Fig. S2 (ESI†).

Discrete model parameters are preserved from Wagner *et al.* (2021)[29] unless specified otherwise in ESI† Section SIC. However, here distinct fractions of stable bonds (with $k_d = 0$) and dynamic bonds (with k_d assigned *a priori*) are randomly and uniformly introduced throughout the networks. The relative fractions of stable and dynamic bonds are assigned as f and $1 - f$, respectively, where $f \in [0,1]$. Note that while the discrete model parameters may be assigned physical units as needed,[41] they are here prescribed in arbitrary normalized units. This is permissible for the purposes of this work, which are to examine the isolated (yet coupled) microstructural evolutions of each bond type, as f is swept, and then relate said microstructures to each chain population's weighted stress. Observations are then used to develop a more general and physically representative continuum approach for application to real-world polymers.

3. A standard rule of mixture for the TNT

While this discrete model permits direct observation of micro-scale statistics, its relatively high computational expense and phenomenological volume exclusion interactions motivate the development of a representative continuum approach (*e.g.*, TNT). TNT predicts the Cauchy stress of a dynamic network comprised entirely of linear entropic springs as:[23,29]

$$\boldsymbol{\sigma} = ck_BT\boldsymbol{\mu} + \pi\boldsymbol{I}, \tag{7}$$

where c is the attached chain concentration, k_B is the Boltzmann constant, T is the ambient temperature, $\pi\boldsymbol{I}$ is the isotropic pressure enforcing elastic incompressibility, and $\boldsymbol{\mu}$ is the conformation tensor whose eigenvalues and eigenvectors define the instantaneous principal magnitudes and directions of average chain stretch, respectively. Supposing constant values of k_d and k_a, the conformation tensor evolves as:‡ [21,23,29,42]

$$\dot{\boldsymbol{\mu}} = \boldsymbol{L}\boldsymbol{\mu} + \boldsymbol{\mu}\boldsymbol{L}^T - k_d(\boldsymbol{\mu} - \boldsymbol{I}). \tag{8}$$

To model networks containing both stable bonds and dynamic bonds, we postulate a general rule of mixture whereby total network stress is given by the weighted sum-of-independent Markov processes governing each bond type's stress response:

$$\boldsymbol{\sigma} = ck_BT[p^s f\boldsymbol{\mu}^s + p^d(1-f)\boldsymbol{\mu}^d] + \pi\boldsymbol{I}, \tag{9}$$

where c is the total chain concentration, while p^s and p^d are the respective probabilities that a given stable or dynamic bond are attached. Note that $\boldsymbol{\mu}^s = \boldsymbol{b}$ becomes the left Cauchy Green tensor for stable bonds ($k_d = 0$). While p^s requires some *a priori* knowledge about the conversion ratio of activated stable bonds, the probability of finding a dynamic bond in the attached state may be approximated as $p^d \approx k_a/(k_a + k_d)$.[23] Applying stress relaxation loading conditions (ESI,† Section SIC), solving for π, and normalizing by the peak stress (see ESI,† Sections SIIA and B for details) gives the normalized stress relaxation response as:

$$\sigma^* = P^{-1}[p^s f + p^d(1-f)e^{-k_d t}], \tag{10}$$

where the normalization factor, $P = p^s f + p^d(1-f)$, enforces that σ^* is unity immediately upon halting the load rate.

Predicted stress from the discrete model and eqn (10) are presented in Fig. 2A for four-armed macromers ($z = 4$), and multiple values of f. The dissociation rate was set such that $k_a \gg k_d$, regardless of f, ensuring that the fraction of attached bonds remained above 95% for all networks (see ESI† Section SIIIA for detailed discussion on the interplay between k_d, k_a, and network connectivity). Here, p^s and p^d were measured from the discrete model (Fig. S4, ESI†). While eqn (10) provides good agreement with discrete model predictions for purely dynamic ($f = 0$) or stable ($f = 1$) networks, it over-predicts the long-term stress for hybrid networks ($0 < f < 1$).

To elucidate the origins of disagreement, we utilize the discrete model to examine the isolated stable bond and dynamic bond characteristics, beginning with the independent probabilities (denoted, respectively, as X^s and X^d) that the stable and dynamic bonds form independently percolated networks.[43] Note that the continuous network formed by both bond types is always percolated for this model, however the probabilities that either bond type forms its own continuous paths spanning the domain bounds varies. Fig. 3A–F display undeformed networks with $f \in \{0.2, 0.5, 0.8\}$, comprised of four-armed ($z = 4$) and eight-armed ($z = 8$) macromers, respectively. When $f < 0.2$, the stable bonds rarely, if ever, form continuous networks (*i.e.*, $X^s \sim 0$) (Fig. 3G and H). Instead, they form clustered regions suspended in a matrix of dynamic bonds (Fig. 3A and D). In contrast, at high f ($f > 0.6$ for $z = 4$ and $f > 0.8$ for $z = 8$), the stable bond networks are always percolated.

One might expect that when the stable bonds percolate through the domain, they will store stress purely elastically, and that eqn (10) will provide good agreement with the network model predictions. Yet Fig. 2A indicates that when $0.8 \leq f < 1$ ($X^s = 1$, Fig. 3G and H) long-term stress is still overpredicted by eqn (10), suggesting that the stable bonds undergo some relaxation. While in physical materials, long-term relaxation

‡ While recent development reveals that eqn (8) is specific to non-incompressible plastic flow, we find that it is a suitable approximation for the conditions of constant average rate kinetics, and intermediate stretches ($\lambda = 2$) used here. Specifically, it yields less than 3% error in principle chain stretch over the updated evolution equation, which gives: $\dot{\boldsymbol{\mu}} = \boldsymbol{L}\boldsymbol{\mu} + \boldsymbol{\mu}\boldsymbol{L}^T - k_d[\boldsymbol{\mu} - 3/\mathrm{tr}(\boldsymbol{\mu}^{-1})\boldsymbol{I}]$.

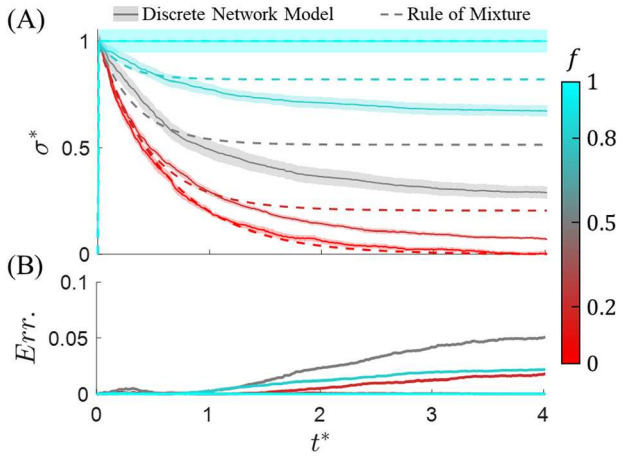

Fig. 2 Fitting the general rule of mixture. (A) Normalized stress, σ^*, is plotted with respect to normalized time, t^*, for the ensemble average of n = 10 discrete network simulations (solid curves with shaded regions representing standard error, S.E.) and as predicted by eqn (10) (dotted curves) when k_d = 1. (B) Absolute errors between the models σ^* are plotted with respect to t^*. (A and B) Results are shown for f = 0% (red), f = 20% (maroon), f = 50% (grey), f = 80% (teal), and f = 100% (cyan). Note that t^* is normalized by the same value of k_d^{-1} for all values of f, such that the timescale is the same for all curves.

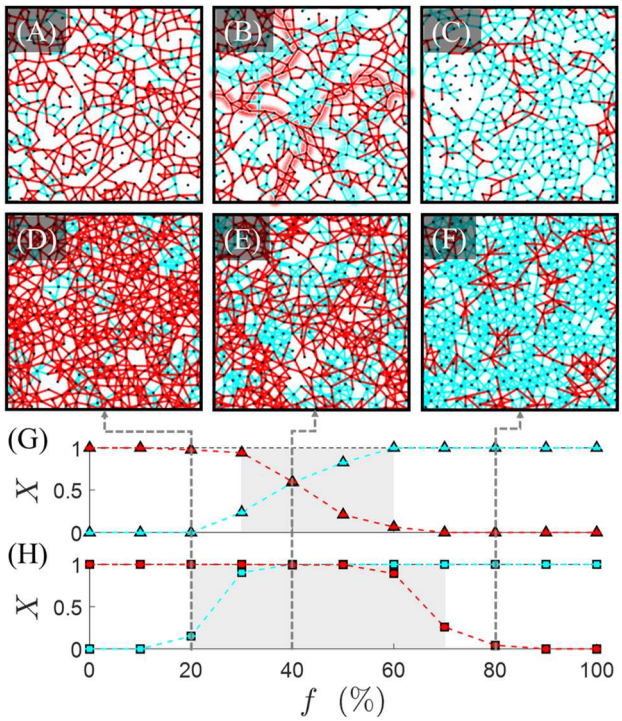

Fig. 3 Network percolation with respect to stable bond fraction and crosslink functionality. (A–C) Sample discrete networks with z = 4 when (A) f = 20%, (B) f = 50%, and (C) f = 80%, illustrate the clustering of (A) stable and (C) dynamic bonds. (B) Dynamic bond paths highlighted by red and stable bond paths highlighted by blue illustrate how under certain conditions (*e.g.*, sufficiently long chain length and high functionality, z), both bond types can form their own percolated load paths. (D–F) Comparable schematics to (A–C) for z = 8 reveal comparable clustering formations. (G) The probability that the stable (cyan) and dynamic (red) bonds independently form geometrically percolated networks (X^s and X^d) are plotted with respect to f for (G) z = 4 and (H) z = 8. (G and H) The regions shaded grey demark transition zones wherein simultaneous, independent percolation of both bond types is possible ($X^s > 0 \cap X^d > 0$). The probability that the dynamic bonds percolate also decreases as the fraction $k_a/(k_a + k_d)$ decreases (Fig. S3–S5, ESI†). (G and H) the region wherein both stable and dynamic bonds can independently percolate (grey) exists over a higher range of mixing fractions, f, and with greater probability for networks with higher coordination (*e.g.*, $X^s \approx X^d \approx 1$ from $f \sim$ 0.4–0.5 for z = 8).

may slow down due to the bond lifetime renormalization effect put forth by Stukalin *et al.* (2013),[33] in the present discrete model, these effects are temporarily ignored to isolate the impact of coupled bond dynamics at intermediate timescales and due to applied strain. The results suggest that conformational degrees of freedom in the stable bonds permit non-affine relaxation modes when inter-connected with dynamic bonds. Indeed, since no relaxation is observed when $f = 1$, it must stem from dynamic bond reconfiguration when $f < 1$.

Furthermore, one might also expect that whenever the stable bonds are discontinuous, their clusters may relax completely such that no long-term stress persists. Yet the network model predicts non-negligible long-term stress when f = 0.2 (Fig. 3A), implying that stable bonds clusters are conformationally constrained by surrounding dynamic bonds. Assuredly, this result is due to the phenomenological choice of steric repulsive interactions and node packing employed in the discrete model, which mitigate non-affine deformations of the stable bonds. Whereas physical polymers will relax at longer timescales due to diffusion and reptation dynamics,[32,44] this simple model neglects these for the time being such that any non-affine relaxation observed is attributed to bond dynamics. Nevertheless, these findings highlight the significant coupling between the stable and dynamic components of network stress, thereby motivating amendment to the rule of mixture.

4. Coupling between bond types mediates relaxation

To amend the rule of mixture we posit that some fraction, ξ, of stable bonds in hybrid networks relax at rate k_d due to reconfiguration of adjacent dynamic bonds, whereas the fraction $1 - \xi$ cannot relax over intermediate timescales because they are constrained by the stable bond network structure, suffer from relaxation retardation due to bond lifetime renormalization effects,[33,35] or are otherwise constrained by steric interactions (as in the case of the 2D, highly packed networks observed in the current discrete model). Incorporating ξ into eqn (9), gives a coupled rule of mixture for hybrid networks:

$$\boldsymbol{\sigma} = ck_BT[(1-\xi)P^s\boldsymbol{b} + \xi P^s\boldsymbol{\mu} + P^d\boldsymbol{\mu}] + \pi\boldsymbol{I}, \qquad (11)$$

where we use $P^s = p^s f$ and $P^d = p^d(1-f)$ for brevity. Solving for π, and normalizing stress (see ESI† Section SIIC for details) gives the relaxation response:

$$\sigma^* = P^{-1}[(1-\xi)P^s + \xi P^s e^{-k_d t} + P^d e^{-k_d t}]. \qquad (12)$$

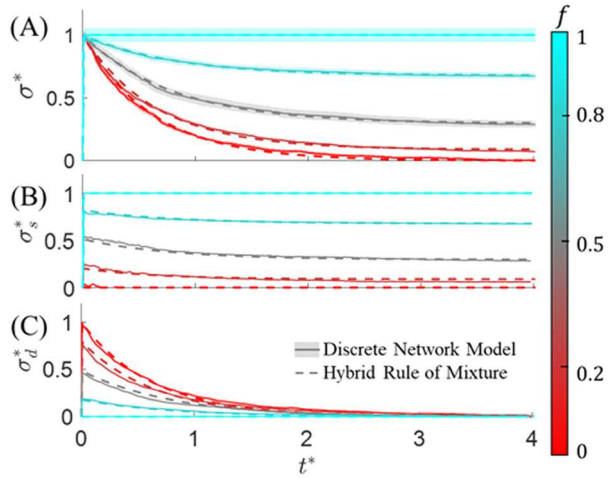

Fig. 4 Fitting the coupled rule of mixture. (A) Normalized stress, σ^*, is plotted with respect to normalized time, t^*, for the ensemble average of $n = 10$ discrete simulations (solid curves with shaded S.E.) and as predicted by eqn (12) (dotted curves) when $k_d = 1$. Stress is decoupled into the contribution from (B) stable bonds, σ_s^*, and (C) dynamic bonds, σ_d^*. Error between models is consistently $<5\%$ at all values of t^* and f. Note that t^* is normalized by the same value of k_d^{-1} for all values of f, such that the timescale is the same for all curves. Regardless, the relaxation timescale remains independent of f (as supported by Fig. S3A and B, ESI†).

When $\xi = 1$, all stable bonds relax completely, and the stress response is purely dynamic whereas when $\xi = 0$, no stable bonds relax and eqn (12) returns the decoupled rule of mixture. The discrete model stress and eqn (12) are in excellent agreement for all values of f when ξ is treated as a fitting parameter (Fig. 4A). Significantly, the isolated stress contributions from the stable (Fig. 4B) and dynamic bonds (Fig. 4C) also agree between models. As confirmed by Fig. S3A or B (ESI†), the relaxation rate remains k_d for all relaxation responses in Fig. 4A–C, regardless of stable bond fraction, f, or bond type. Therefore, the only major difference between curves in Fig. 4A or B is the extent (and not timescale) of stress decay. Furthermore, Fig. S3A and B (ESI†) confirm that the values of k_d (i) set *a priori* in the discrete model, (ii) emerging stochastically from the discrete model, and (iii) fitted to the discrete data with the continuum model are all in good agreement indicating consistency between approaches. With this confirmed, we may interpret the isolated stress responses of each bond type.

Fig. 4C confirms that isolated dynamic bond stress from both models decays exponentially to zero stress at a rate of k_d, in all networks. This indicates that only stable bond relaxation is significantly affected by coupling in the discrete model and justifies the way in which the second term of eqn (12) depends only on the stable bond fraction (through P^s). Furthermore, it supports the presumption that, ignoring short term α-relaxation[45]

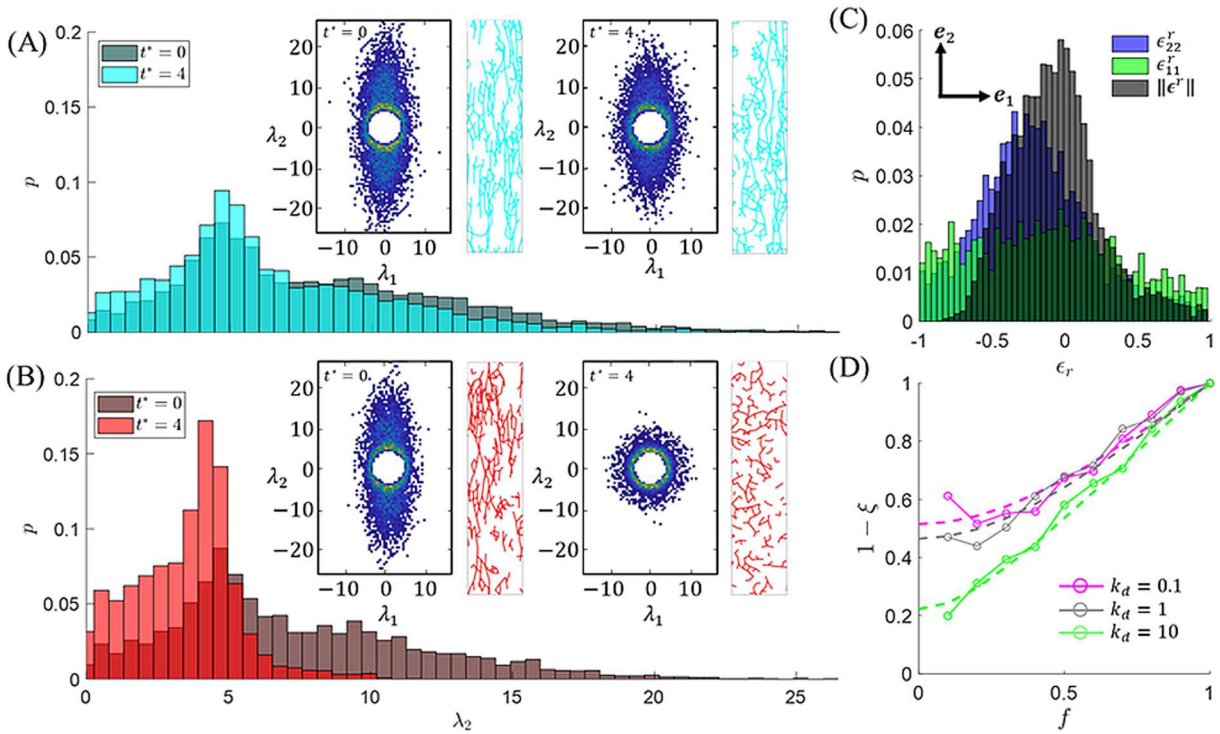

Fig. 5 Topological relaxation data. (A and B) The PMFs of (A) stable and (B) dynamic bond end-to-end stretch, λ, at $t^* = 0$ and $t^* = 4$. Insets of (A and B) display the joint (*i.e.*, 2D) PMFs of the respective bond types and the visually isolated stable and dynamic bond networks, also at times $t^* = 0$ and $t^* = 4$. (C) The PMFs of $\varepsilon_{22}^r = (r_2 - r_2^0)/r_2^0$ (blue), $\varepsilon_{11}^r = (r_1 - r_1^0)/r_1^0$ (green), and $\|\boldsymbol{\varepsilon}^r\| = (|\boldsymbol{r}| - |\boldsymbol{r}_0|)/|\boldsymbol{r}_0|$ (black) are presented where $\boldsymbol{r}^0$ and $\boldsymbol{r}$ are the end-to-end vectors of stable bonds at times $t^* = 0$ and $t^* = 4$, respectively. (D) Fitted values of $1 - \xi$ are plotted with respect to f for three different values of k_d. Discrete circles represent the results of the network model, while dashed curves represent fitted functions per eqn (13) where $\eta = 0.52$ for $k_d = 0.1$ (magenta, $R^2 = 0.94$), $\eta = 0.46$ for $k_d = 0.1$ (grey, $R^2 = 0.96$), and $\eta = 0.22$ for $k_d = 10$ (magenta, $R^2 = 0.99$).

(which is not modeled on the basis of very fast short term segmental relaxation[45,46]), bond types with faster dissociation kinetics in multi-bond-type networks dominate the reconfiguration-driven relaxation response.[17] Fig. 4B confirms that stable bond stress predictions agree between models, and that ξ characterizes the extent to which stable bonds conform non-affinely into lower energy states at a rate of k_d (Fig. 4B). However, it is not immediately clear whether ξ defines a fraction of stable bonds that relax entirely, the degree to which all stable bonds relax partially, or some combination of both. To elucidate the meaning of ξ, as it applies to the network model, we leverage directly measured discrete topological data.

Fig. 5A and B illustrate the probability mass functions (PMFs) of stable and dynamic bonds end-to-end stretches, $\boldsymbol{\lambda} = \boldsymbol{r}/(\sqrt{N}b)$, in the principal direction of loading at the start and end of relaxation (f = 0.5). The insets display the 2D PMFs of chain stretch, along with isolated network snapshots at the start and end of relaxation. As evidenced by the axisymmetric 2D PMF of Fig. 5B (t^* = 4), dynamic bonds reconfigure completely to an isotropic state, whereas the elongated 2D PMF and diminished reduction in variance from Fig. 5A confirm that stable bond relaxation is partial. To quantify modes of stable bond relaxation, Fig. 5C presents the distributions of single-chain relaxation strains, $\boldsymbol{\varepsilon}^r$, in the principal directions of the orthonormal basis $\{\boldsymbol{e}_1, \boldsymbol{e}_2\}$, and the change in end-to-end norms, $\|\boldsymbol{\varepsilon}^r\|$. Notably, some stable bonds elongate ($\|\boldsymbol{\varepsilon}^r\| > 0$), indicating that thermal fluctuations stochastically move a minority of stable bonds to temporarily higher energy states. However, most stable bonds relax into lower energy states ($\|\boldsymbol{\varepsilon}^r\| < 0$), and shorten in the direction of principal stretch, $\boldsymbol{e}_2$. In contrast, stable bonds undergo roughly equiprobable shortening or lengthening in direction $\boldsymbol{e}_1$. Lengthening in $\boldsymbol{e}_1$ can occur due to chain stretching but is confirmed to occur predominantly due to reorientation.

Fig. 5C confirms that most stable bonds relaxed, but to a variable degree. Therefore, ξ cannot be mapped to a single, physical value, rather it lumps the effects of stable bond shortening and reorientation into some effective scalar. Nevertheless, we seek to understand how ξ evolves with respect to f. First, we recognize that no stable bond relaxation occurs in permanent networks (*i.e.*, $\xi(f = 1) = 0$). We also observe that, some fraction of stable bonds, η, may fail to relax even in the limit $f \to 0$ (consistent with studies of highly packed granular networks that jam through exclusively repulsive forces[47,48] or polymers that exists below their glass transition state due to low free volume[49]). Motivated by these observations, we introduce a simple phenomenological scaling rule that gives the degree of stable relaxation as:

$$\xi \sim 1 - \sqrt{\eta^2 + f^2(1 - \eta^2)}. \quad (13)$$

When η = 1 (*i.e.*, no stable bonds relax, even in the limit $f \to 0$), eqn (13) devolves into $\xi \sim 1$ regardless of the stable bond fraction, f. This states that if a network of entirely dynamic bonds deforms affinely and fails to relax stress, then so too will networks containing increasingly large fractions of stable bonds. In contrast, when η = 0 (indicative of full stable bond relaxation for $f \to 0$, which is likely more representative of polymers), eqn (13) devolves to $\xi \sim 1 - f$ suggesting that the fraction of stable bonds that relax over intermediate timescales is proportionate to the relative compositional fraction of dynamic bonds in the overall network (as seen in the following section for an experimentally tested gel).

Fig. 5D depicts the degree of stable bond non-relaxation, $1 - \xi$, with respect to $f \in (0,1]$ for $k_d \in \{0.1,1,10\}$ and z = 4. As f increases, $1 - \xi$ increases, implying that percolation of stable bonds inhibits their relaxation. This interpretation is further supported by the fact that networks with higher coordination (begetting greater stable bond percolation) display $(1 - \xi)$-*versus*-f relations that extrapolate to greater values of η (Fig. S6, ESI†). Surprisingly, networks in which stable bond percolation is enhanced by increased chain length – although well-represented by eqn (12) – do not exhibit higher η suggesting a diminishing effect of stable bond percolation on relaxation inhibition. Notably, without sufficient network connectivity (*e.g.*, for short chain networks, Fig. S7 and S8, ESI†), the coupled rule of mixture cannot accurately predict stable bond relaxation, as it becomes dominated by floppy deformation modes[43] at shorter timescales.

Another factor influencing network percolation is dynamic bond reaction rates. Networks with higher k_d generally demonstrate greater stable bond relaxation in the limit $f \to 0$ (η = 0.52 for k_d = 0.1 whereas η = 0.22 for k_d = 10) (Fig. 5D). Since all networks relaxed for $t^* = t/k_d = 4$, one might expect identical behavior regardless of k_d. However, the parameters governing k_a are preserved across simulations so that the steady state fraction of attached dynamic bonds ($p^d \approx k_a/(k_a + k_d)$), decreases as k_d increases. This indicates that η is correlated with p^d and suggests that networks in which $k_a \gg k_d$ mitigate conformational change of stable bonds to a greater extent in a manner that supports the concept of bond lifetime renormalization discussed in the following section.[33]

It must be noted that the failure of stable bonds to relax below their independent percolation threshold is here attributable to steric interactions arising from the phenomenological pairwise repulsive potential, node packing, and 2D conditions utilized in the discrete network. Lowering the degree of repulsion or node density, as well as implementing the model in 3D, would inhibit this effect by increasing the networks' effective free volumes.[49] While reduced chain mobilization is certainly observable in polymers below glass transition conditions (*e.g.*, low temperature and free volume), even glassy polymers are expected to relax residual stress over longer timescales at rates inversely related to polymer packing and inter-chain interaction strength.[50–52] Therefore, the discrete model is not representative of long term relaxation, but rather usefully elucidates the effects of bond kinetics at intermediate timescales (above the timescale of short term α-relaxation[35] but below the timescale of reptation[32]). Nevertheless, the concept of finite η within polymeric networks is seemingly non-physical and in the remainder of this work η = 0 (*i.e.*, $\xi \sim 1 - f$) is observed.

5. Coupling effects on dynamic hydrogel relaxation

To exhibit the utility of the coupled rule of mixture, we apply it to the stress relaxation data provided by Richardson *et al.* (2019)[6] for hydrazone covalently adaptable, 8-arm, poly(ethylene glycol)-based hydrogels. These gels contain "slower" and "faster" benzyl-hydrazone (bHz) and alkyl–hydrazone (aHz) bonds with kinetic dissociation rates of k_β and k_α, respectively. Here, k_α and k_β are not to be confused with the attachment rate, k_a, or Boltzmann constant, k_B, described in prior sections. Based on the experiments' use of parallel plate rheometry, eqn (12) is rederived for simple shear conditions as:

$$\sigma^* = P^{-1}[(1-\xi)P^\beta e^{-k_\beta t} + \xi P^\beta e^{-k_\alpha t} + P^\alpha e^{-k_\alpha t}], \quad (14)$$

where $P^\beta = fp^\beta$ and $P^\alpha = (f-1)p^\alpha$; f is the fraction of bHz; and p^β and p^α are the attached fractions of bHz and aHz, respectively ($p^\beta = p^\alpha > 0.9$ assuming network equilibrium is met before strain is applied and that the attachment rate is much greater than the detachment rate) (see ESI† Section SIID for detailed derivations). Significantly, we have again postulated that the coupled stress term relaxes at the faster of the two kinetic rates, k_α.[17]

As indicated by Richardson *et al.* (2019),[6] and evidenced by non-exponential relaxation curves for $f = \{0,1\}$ (Fig. 6A), bHz and aHz bonds exhibit slower relaxation at longer timescales than immediately after strain is applied. While a similarly observed effect in the discrete network model is attributed to a low free volume-induced, glassy-like state, a more suitable explanation for this behavior in gels is the bond lifetime renormalization effect proposed by Stukalin *et al.* (2013),[33] which posits that reversible bonds – while detaching at some mean thermodynamic rate according to an Arrhenius type equation[35,53] – relax network stress only as fast as they may attach into new configurations. Essentially, the renormalized bond lifetime accounts for functional end groups' tendencies to repeatedly dissociate and associate with the same neighboring chains before diffusing through sufficient space to bind into lower energy states, thereby retarding the long-tail relaxation rate. We here incorporate bond lifetime renormalization into the continuum framework per the details of ESI† Section SIIE.

To fit the non-exponential relaxation of the experimental data, we find that we must also account for the change in polymer chains' free energies as they are extended beyond their mean equilibrium stretch of $\lambda = 1$ (where $\lambda = r/(\sqrt{N}b)$ for Gaussian chains[29]). Following Eyring's supposition that intrinsic bond lifetime within complex polymer systems decreases with increasing chain force,[54] we utilize Bell's model[36,55–57] that gives the force-adjusted bond lifetime according to:

$$\tau_i = \tau_0 \exp\left(\frac{\varepsilon_i - f_t \Delta x}{k_B T}\right), \quad (15)$$

where $i \in \{\alpha, \beta\}$ denotes either aHz or bHz; τ_0 remains the time it takes a single Kuhn segment to diffuse its own length, b; ε_α and ε_β are the bond activation energies of aHz and bHz, respectively; f_t is the single chain force from eqn (3); Δx is the reaction coordinate characterizing the distance from the equilibrium bond length to the activation barrier; k_B is the Boltzmann constant; and T is temperature.

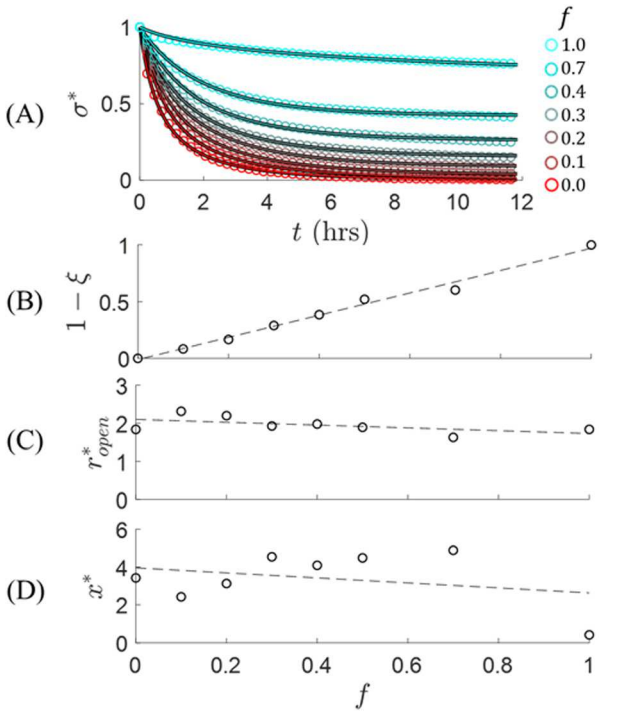

Fig. 6 Experimental validation. (A) The coupled rule of mixture with bond lifetime renormalization and force-dependent bond dissociation (solid curves) is fit to the experimental stress relaxation data (circles) for hydrazone covalently adaptable network with $f \in \{0, 10, 20, 30, 40, 70, 100\}$% bHz. $f = 0$ is represented by red and $f = 1$ is represented by cyan. $R^2 > 0.99$ for all values of f. Experimental data adapted from Richardson *et al.* (2019). (B) Fitted values of $1-\xi$ (black circles) are plotted with respect to f. The dotted curve represents the scaling relation $1-\xi \sim f$ (with a correlation coefficient of $R = 0.99$). (C and D) The normalized distance between open stickers, r^*_{open} and bond activation length scale, x^*, are plotted against f, respectively. The dotted curves represent the fits from linear regression analysis giving correlation coefficients of $R = -0.56$ and $R = -0.30$, respectively.

Accounting for both bond lifetime renormalization and force-adjusted bond dissociation kinetics through eqn (15) (see ESI† Section SIIE for details) gives the effective relaxation rate of each respective bond type as:

$$k_\alpha \approx \frac{\left[c^*_{open}(1-f)\right]^{1/3}}{\tau_0}\left[K^0_\alpha \exp\left(-\sqrt{\frac{\sigma^*}{\sigma^*_0}}\right) + \frac{1}{c^*_{open}(1-f)}\right]^{-1}, \quad (16)$$

and:

$$k_\beta \approx \frac{\left(c^*_{open} f\right)^{1/3}}{\tau_0}\left[K^0_\beta \exp\left(-\sqrt{\frac{\sigma^*}{\sigma^*_0}}\right) + \frac{1}{c^*_{open} f}\right]^{-1}, \quad (17)$$

where $c^*_{open} = b^3 c_{open}$ is the total open sticker concentration, c_{open}, normalized by the characteristic Kuhn volume, b^3; $K_i^0 = \exp(\varepsilon_i/k_B T)$ is the dissociation kinetic constant of bond type $i \in \{\alpha, \beta\}$ when it connects a chain at the equilibrium stretch (such

that the force-free bond lifetime is $K_i^0\tau_0$); and σ_0^* defines the intrinsic bond dissociation rates sensitivity to internal stress, where $\sigma_0^* \to \infty$ begets stress invariance. Analytically, σ_0^* is treated as a fitting parameter but it is related to the bond reaction coordinate length, Δx, by:

$$\Delta x = b\sqrt{\frac{N\,\sin(2\gamma)}{3p\gamma}\sigma_0^*}, \tag{18}$$

where N = 88 is the approximate number of Kuhn segments of length b = 0.78 nm, based on the molecular weight of the 8-armed, star-shaped macromers used in experiments (M_w = 8000 g mol^{-1}) and that of ethylene glycol (M_{eg} = 44.05 g mol^{-1}). Furthermore, $p \approx p^\beta \approx p^\alpha > 0.9$ is the fraction of attached chains and γ = 0.1 is the experimentally applied shear strain magnitude.[6,41] Note that through eqn (16) and (17), the relaxation rate goes to zero when the open sticker concentration or bond fraction (f for bHz and $1 - f$ for aHz) of the corresponding bond type is zero.

This model has five dimensionless free parameters, K_α^0, K_β^0, c_{open}^*, σ_0^*, and ξ as well as a fifth unknown parameter, τ_0. While c_{open}^*, σ_0^*, and ξ are liable to change with respect to the relative bond fraction, K_α^0 and K_β^0 are intrinsic constants associated with aHz and bHz bonds, respectively. Furthermore, τ_0 is the timescale of monomer diffusion treated as identical between functional groups since they are on the same order molecular weight. Therefore, the steps used to fit the model parameters are as follows:

1. Fit the normalized stress *versus* time for the purely aHz network with τ_0, K_α^0, c_{open}^*, and σ_0^* as the fitting parameters (since ξ = 0 without bHz present). K_α^0 is then fixed moving forward for any networks containing aHz.

2. Fixing τ_0, fit the normalized stress *versus* time for the purely bHz network with K_β^0, c_{open}^*, and σ_0^* as the only fitting parameters (since $\xi \approx 1$ for a network comprised of bHz). K_β^0 is fixed moving forward for networks containing bHz.

3. Fit the remainder of the mixed networks' stress responses with σ_0^*, c_{open}^*, and ξ treated as free parameters.

Fitting the parameters per the procedure above and the methods detailed in ESI† Section SIIF, the model predicts that the timescale of tethered monomer diffusion is on the order of 20 μs (consistent with the segmental relaxation timescale of comparable telechelic bond groups such as poly(isobutylene) at room temperature).[46] It also predicts that the bond activation energies of aHz and bHz are $\varepsilon_\alpha = k_B T \ln K_\alpha^0 \approx$ 38.5 kJ mol^{-1} and $\varepsilon_\beta = k_B T \ln K_\beta^0 \approx$ 85.7 kJ mol^{-1}, respectively (where an ambient temperature of $T \approx$ 293 K is assumed). For comparison, the activation energy of hydrogen bonding in water is on the order of 18 kJ mol^{-1} while that of single carbon–carbon bond is upwards 271 kJ mol^{-1} indicating that the model predicts realistic values.[58,59] Indeed, fixing these values while treating ξ, c_{open}^*, and σ_0^* as fitting parameters for the mixed networks, the coupled rule of mixture predicts stress responses in excellent agreement ($R^2 > 0.99$) with the experimental data (Fig. 6A).

Fitted values of the bHz non-relaxation degree ($1 - \xi$), average normalized distance between open stickers ($r_{open}^* = c_{open}{}^{-1/3}/Nb$), and normalized bond reaction coordinate length ($x^* = \Delta x/b$ through eqn (18)) are presented in Fig. 6B–D, respectively. The values of r_{open}^* (Fig. 6C) suggest that the distance between open stickers is believably on the order of a chains contour length (here, $Nb \approx$ 70 nm). Specifically, $r_{open}^* \sim 2$ indicating that most open stickers are not within reach of adjacent open sites and thus partially explaining the appearance of slower relaxation rates over longer timescales. Interpreting x^* (Fig. 6D), we see that the reaction coordinate length scale is roughly on the order of two to four Kuhn lengths (where b = 0.78 nm) suggesting that the distance between the minimum energetic spacing and the transition length is on the order of 1.6 to 3.2 nm. Alternatively, recognizing through eqn (3) and (15) that the dissociation rate for either species may be written as $k_i = k_i^0 \exp(3\lambda x^*/\sqrt{N})$, then $\lambda_0 = \sqrt{N}/3x^*$ is the stretch at which the dissociation rate increases by a factor of e^1 as compared to the force-free rate, $k_i^0 = (K_i^0\tau_0)^{-1}$. On average, this occurs at a predicted chain stretch of λ = 1.8. Note that, while we here simply treat x^* as a single fitting parameter for both species, more accurate fitting is attainable by decoupling this length scale for aHz and bHz. However, we find that decoupling Δx for both bond types into separate parameters does not significantly impact the relation between ξ and f (the primary focus of this work).

Significantly, neither r_{open}^* nor x^* are strongly correlated with the fraction of stable bonds, f. Thus, while still significant for the non-exponential relaxation response observed across all hybrid networks, bond lifetime renormalization and force-sensitive bond dissociation are not the primary factors influencing differences observed between these samples. In contrast, the degree of bHz non-relaxation, $1 - \xi$, is strongly correlated with f, justifying the choice of scaling through eqn (13), under the condition that $\eta \to 0$ and $\xi \approx 1 - f$.§ Furthermore, it proves necessary to account for some degree of stable bond relaxation through ξ to fit the observed stress response. In other words, a standard rule of mixture – presuming that all bHz relax no faster than the rate allowed by k_β – does not predict the correct mechanical response. Together, the necessity of including the coupled rule of mixture and the strong correlation between $1 - \xi$ and f, suggest that the degree of coupled relaxation is a significant effect governing the observed trends as the relative fractions of each bond type are swept in this model hydrogel.

6. Conclusion

Here we utilized a network model to explore coupled stress response of networks containing multiple bond types within one continuous network. We discovered that for a simple 2D network model whose only relaxation timescale is governed by bond dynamics, long-term moduli may subsist at low stable

§ As mentioned previously, finite values of η are not expected for polymeric systems wherein reptation and Rouse diffusion ensure relaxation, especially for swollen gels whose polymer volume fractions are on the order of 0.01–0.1.[41]

bond fractions due to low free volume and hinderance of stable chain reptation. However, this result is specific to the phenomenological repulsive potentials, high packing fractions, and 2D framework employed in the discrete network model such that it is not expected to hold in 3D frameworks or real-world systems. Indeed, stored stress in even tightly packed polymer systems decays at longer timescales due to segmental relaxation and reptation.[34] Meanwhile, long-term moduli of polymers with high free volumes (*e.g.*, swollen gels) are likely unaffected by inter-chain topological volume exclusion. This result nevertheless emphasizes the important influence that network topology has on stable chains segmental relaxation. A more representative finding of the network model is that even stable bonds may undergo non-affine, conformational stress relaxation over intermediate timescales due to adjacent dynamic bond reconfiguration. Notably, the rate of stable bond relaxation in the discrete model – whose only source of stress relaxation is stochastic bond exchange – coincides with that of the prescribed dynamic bond dissociation. These effects motivated the introduction of a novel, dimensionless coupling parameter, ξ, that weights the degree of stable bond relaxation at rate k_d and which inversely correlates with the stable bond fraction, f. Incorporating this parameter into TNT, we developed a coupled rule of mixture for hybrid dynamic networks.

Significantly, the discrete model is a deliberate idealization formulated to isolate the effects of bond kinetics, thereby neglecting other first-order physical effects such as polydispersity, segmental relaxation,[35,45] poroelastic relaxation,[60] damage-induced dissipation,[61,62] long-term hydrolysis/degradation,[63,64] or reptation.[32,44] These additional confounding factors emphasize that coupling the relaxation between separate bond types is, on its own, not sufficient to encapsulate the complex dissipative behavior of polymeric systems. Nevertheless, to demonstrate the importance of bond coupling, we employed the coupled rule of mixture through TNT to model the mechanical response of physical gel networks hosting two, reversible hydrazone bond types. To account for experimentally observed strain-dependent relaxation times,[36,54,55,65] we concurrently considered the effects of relaxation-retarding bond lifetime renormalization[33,35] and relaxation-enhancing force-sensitive dissociation.[6,36] The model predicts that the concentrations of open binding sites (governing bond lifetime renormalization) and the reaction coordinate length (governing the sensitivity of force-dependent bond dissociation) are only weakly correlated with f. However, the coupling parameter (dictating the degree of relatively stable bond relaxation due to kinetics of more dynamic bonds) is highly correlated with f. This provides strong evidence that inter-bond coupling is a dominant effect that researchers should consider when investigating networks with controlled fractions of mixed bond types. The simplicity and robustness of this approach, combined with its compatibility with other first-order physical phenomena, may render it useful for predictive design of diverse hybrid networks including elastomers with charge interactions,[16,65,66] vitrimers,[6] and metallopolymers.[7,9] Therefore, in future work, this method may be utilized in conjunction with additional modeling approaches for other significant phenomena (*e.g.*, entanglement, reptation, *etc.*) to investigate polymer micromechanics or guide design applications.

Author contributions

R. J. W. conceptualization, methodology, software, validation, formal analysis, investigation, data curation, writing – original draft, writing – review & editing, visualization. F. J. V. conceptualization, resources, supervision, project administration, funding acquisition.

Conflicts of interest

There are no conflicts to declare.

Acknowledgements

The authors gratefully acknowledge the support of the National Science Foundation (NSF) under award no. 2029699. This content is solely the responsibility of the authors and does not necessarily represent the official views of NSF.

Notes and references

1 J. Gong, Y. Katsuyama, T. Kurokawa and Y. Osada, *Adv. Mater.*, 2003, **15**, 1155–1158.
2 E. Ducrot, Y. Chen, M. Bulters, R. P. Sijbesma and C. Creton, *Science*, 2014, **344**, 186–189.
3 A. E. Elbanna and J. M. Carlson, *PLoS One*, 2013, **8**, e56118.
4 K. Mayumi, J. Guo, T. Narita, C. Y. Hui and C. Creton, *Extreme Mech. Lett.*, 2016, **6**, 52–59.
5 Y. Chen, G. Sanoja and C. Creton, *Chem. Sci.*, 2021, **12**, 11098–11108.
6 B. M. Richardson, D. G. Wilcox, M. A. Randolph and K. S. Anseth, *Acta Biomater.*, 2019, **83**, 71–82.
7 Y. Vidavsky, M. R. Buche, Z. M. Sparrow, X. Zhang, S. J. Yang, R. A. J. DiStasio and M. N. Silberstein, *Macromolecules*, 2020, **53**, 2021–2030.
8 Y. Vidavsky, S. Bae and M. N. Silberstein, *J. Polym. Sci., Part A: Polym. Chem.*, 2018, **56**, 1117–1122.
9 L. Xu, Y. Fu, R. J. Wagner, X. Zou, Q. He, T. Li, W. Pan, J. Ding and F. J. Vernerey, *Macromol. Rapid Commun.*, 2022, **43**, 2200320.
10 Z. Song, Z. Wang and S. Cai, *Mech. Mater.*, 2021, **153**, 103687.
11 X. Li, K. Cui, T. L. Sun, L. Meng, C. Yu, L. Li, C. Creton, T. Kurokawa and J. P. Gong, *Proc. Natl. Acad. Sci. U. S. A.*, 2020, **117**, 7606–7612.
12 N. S. Schauser, G. E. Sanoja, J. M. Bartels, S. K. Jain, J. G. Hu, S. Han, L. M. Walker, M. E. Helgeson, R. Seshadri and R. A. Segalman, *Chem. Mater.*, 2018, **30**, 5759–5769.
13 G. Foyart, C. Ligoure, S. Mora and L. Ramos, *ACS Macro Lett.*, 2016, **5**, 1080–1083.

14 M. Gianneli, P. W. Beines, R. F. Roskamp, K. Koynov, G. Fytas and W. Knoll, *J. Phys. Chem. C*, 2007, **111**, 13205–13211.
15 S. Lalitha Sridhar and F. J. Vernerey, *J. Mech. Phys. Solids*, 2020, **141**, 104021.
16 H. Chen, J. Zhang, W. Yu, Y. Cao, Z. Cao and Y. Tan, *Angew. Chem., Int. Ed.*, 2021, **60**, 22332–22338.
17 L. Porath, J. Huang, N. Ramlawi, M. Derkaloustian, R. H. Ewoldt and C. M. Evans, *Macromolecules*, 2022, **55**, 4450–4458.
18 G. I. Dzhardimalieva, B. C. Yadav, S. Singh and I. E. Uflyand, *Dalton Trans.*, 2020, **49**, 3042–3087.
19 N. Roy, B. Bruchmann and J.-M. Lehn, *Chem. Soc. Rev.*, 2015, **44**, 3786–3807.
20 S. Mora, *Soft Matter*, 2011, **7**, 4908–4917.
21 T. Shen and F. J. Vernerey, *J. Mech. Phys. Solids*, 2020, **143**, 104028.
22 F. Tanaka and S. F. Edwards, *Macromolecules*, 1992, **25**, 1516–1523.
23 F. J. Vernerey, R. Long and R. Brighenti, *J. Mech. Phys. Solids*, 2017, **107**, 1–20.
24 T. Matsunaga, T. Sakai, Y. Akagi, U.-I. Chung and M. Shibayama, *Macromolecules*, 2009, **42**, 6245–6252.
25 J. Karvinen, T. O. Ihalainen, M. T. Calejo, I. Jönkkäri and M. Kellomäki, *Mater. Sci. Eng., C*, 2019, **94**, 1056–1066.
26 X. Li and C. Reina, *J. Mech. Phys. Solids*, 2019, **130**, 118–140.
27 A. Sugimura, M. Asai, T. Matsunaga, Y. Akagi, T. Sakai, H. Noguchi and M. Shibayama, *Polym. J.*, 2013, **45**, 300–306.
28 K. Kothari, Y. Hu, S. Gupta and A. Elbanna, *J. Appl. Mech.*, 2018, **85**, 031008.
29 R. J. Wagner, E. Hobbs and F. J. Vernerey, *Soft Matter*, 2021, **17**, 8742–8757.
30 N. Cohen, C. Du and Z. L. Wu, *Macromolecules*, 2021, **54**, 11316–11325.
31 T. Leadbetter, A. Seiphoori, C. Reina and P. K. Purohit, *J. Mech. Phys. Solids*, 2022, **158**, 104660.
32 G. Marrucci, *J. Polym. Sci., Polym. Phys. Ed.*, 1985, **23**, 159–177.
33 E. B. Stukalin, L.-H. Cai, N. A. Kumar, L. Leibler and M. Rubinstein, *Macromolecules*, 2013, **46**, 7525–7541.
34 L. Leibler, M. Rubinstein and R. H. Colby, *Macromolecules*, 1991, **24**, 4701–4707.
35 S. Ge, M. Tress, K. Xing, P.-F. Cao, T. Saito and A. P. Sokolov, *Soft Matter*, 2020, **16**, 390–401.
36 Z. Song, T. Shen, F. J. Vernerey and S. Cai, *Soft Matter*, 2021, **17**, 6669–6674.
37 S. Ahmadi, M. Schmidt, R. J. Spiteri and R. K. Bowles, *J. Chem. Phys.*, 2019, **150**, 224501.
38 J. C. Meza, *Wiley Interdiscip. Rev. Comput. Stat.*, 2010, **2**, 719–722.
39 A. Einstein, *Ann. Phys.*, 1905, **322**, 549–560.
40 W. Sutherland, *London Edinburgh Philos. Mag. J. Sci.*, 1905, **9**, 781–785.
41 R. J. Wagner, J. Dai, X. Su and F. J. Vernerey, *J. Mech. Phys. Solids*, 2022, **167**, 104982.
42 T. Shen, Z. Song, S. Cai and F. J. Vernerey, *Proc. Natl. Acad. Sci. U. S. A.*, 2021, **118**, e2105974118.
43 R. C. Picu, *Soft Matter*, 2011, **7**, 6768–6785.
44 P. G. de Gennes, *J. Chem. Phys.*, 1971, **55**, 572–579.
45 K. Chen, E. J. Saltzman and K. S. Schweizer, *J. Phys.: Condens. Matter*, 2009, **21**, 503101.
46 A. Mordvinkin, D. Döhler, W. H. Binder, R. H. Colby and K. Saalwächter, *Macromolecules*, 2021, **54**, 5065–5076.
47 R. P. Behringer, *C. R. Phys.*, 2015, **16**, 10–25.
48 R. P. Behringer and B. Chakraborty, *Rep. Prog. Phys.*, 2018, **82**, 012601.
49 R. P. White and J. E. G. Lipson, *Macromolecules*, 2016, **49**, 3987–4007.
50 R. Minguez, L. Barrenetxea, E. Solaberrieta and E. Lizundia, *Eur. J. Phys.*, 2018, **40**, 015502.
51 L. J. Fetters, D. J. Lohse, S. T. Milner and W. W. Graessley, *Macromolecules*, 1999, **32**, 6847–6851.
52 T. Inoue, T. Uematsu, Y. Yamashita and K. Osaki, *Macromolecules*, 2002, **35**, 4718–4724.
53 H. Eyring, *Chem. Rev.*, 1935, **17**, 65–77.
54 W. Kauzmann and H. Eyring, *J. Am. Chem. Soc.*, 1940, **62**, 3113–3125.
55 G. I. Bell, *Science*, 1978, **200**, 618–627.
56 E. Evans and K. Ritchie, *Biophys. J.*, 1997, **72**, 1541–1555.
57 F. Meng, R. H. Pritchard and E. M. Terentjev, *Macromolecules*, 2016, **49**, 2843–2852.
58 R. Mills, *J. Phys. Chem.*, 1973, **77**, 685–688.
59 L. S. Kassel, *Nature*, 1930, **125**, 926.
60 Y. Hu and Z. Suo, *Acta Mech. Solida Sin.*, 2012, **25**, 441–458.
61 S. C. Lamont, J. Mulderrig, N. Bouklas and F. J. Vernerey, *Macromolecules*, 2021, **54**, 10801–10813.
62 F. J. Vernerey, R. Brighenti, R. Long and T. Shen, *Macromolecules*, 2018, **51**, 6609–6622.
63 K. Dey, S. Agnelli, E. Borsani and L. Sartore, *Gels*, 2021, **7**, 277.
64 J. Kalia and R. T. Raines, *Angew. Chem., Int. Ed.*, 2008, **47**, 7523–7526.
65 Y. Li, A. Nese, K. Matyjaszewski and S. S. Sheiko, *Macromolecules*, 2013, **46**, 7196–7201.
66 T. L. Sun, T. Kurokawa, S. Kuroda, A. B. Ihsan, T. Akasaki, K. Sato, M. A. Haque, T. Nakajima and J. P. Gong, *Nat. Mater.*, 2013, **12**, 932–937.

